

Journal of Materials Chemistry A

Accepted Manuscript



This is an *Accepted Manuscript*, which has been through the Royal Society of Chemistry peer review process and has been accepted for publication.

Accepted Manuscripts are published online shortly after acceptance, before technical editing, formatting and proof reading. Using this free service, authors can make their results available to the community, in citable form, before we publish the edited article. We will replace this *Accepted Manuscript* with the edited and formatted *Advance Article* as soon as it is available.

You can find more information about *Accepted Manuscripts* in the [Information for Authors](#).

Please note that technical editing may introduce minor changes to the text and/or graphics, which may alter content. The journal's standard [Terms & Conditions](#) and the [Ethical guidelines](#) still apply. In no event shall the Royal Society of Chemistry be held responsible for any errors or omissions in this *Accepted Manuscript* or any consequences arising from the use of any information it contains.

Cite this: DOI: 10.1039/c0xx00000x

www.rsc.org/xxxxxx

ARTICLE TYPE

Synthesis and characterizations of Mn-based compositing oxides with enhanced electrocatalytic activity for oxygen reduction

Yin Xu,^a Haochen Jiang,^a Xiaoxiao Li,^a Han Xiao,^a Wei Xiao^{*a} and Tian Wu^{*b}*Received (in XXX, XXX) Xth XXXXXXXXXX 20XX, Accepted Xth XXXXXXXXXX 20XX*

DOI: 10.1039/b000000x

Implementation of non-precious electrocatalysts towards the Oxygen Reduction Reaction (ORR) falls in the central focus on fulfilling cost-affordable and high-performance fuel cells and metal/air batteries. Herein, we report a modified solvothermal approach for preparation of compositing carbonates between Mn and X (X= Co, Ni and Fe). Upon a post annealing treatment, the aforesaid carbonates are transformed into the corresponding micro/nano hierarchical structured mixed oxides with increase in porosity. It is found that onion-like core-shell architectures appear in the Mn-Co and Mn-Ni systems due to the volume shrinkage arisen from the generation of chemical-level mixed oxides. While less porous structure occurs in the Mn-Fe system with the formation of a physical-level mixture. The ORR activity of the prepared compositing oxides in alkaline media are investigated by voltammetry in different hydrodynamic conditions. An enhanced ORR activity is observed in the Mn-Co mixed oxide, which is rationalized in terms of the unique microstructure and crystallographic phase. The present study suggests that proper mixing is an effective method on activating ORR activity of manganese oxides, which is beneficial to developing non-precious electrocatalysts for fuel cells and metal/air batteries.

Introduction

We are now forced to stand in the transition from heavy dependence on fossil fuels to more green and renewable energy solutions due to the inevitable depletion of fossil fuels and intensive environmental concerns on combustion of fossil fuels. Electrochemical energy storage/conversion devices such as batteries, fuel cells and supercapacitors are highly regarded in response to the aforesaid energy and environmental issues due to the employment of green and no-trace electrons as energy carriers, and technological maturation of electricity industries. Although rechargeable batteries, e.g. lithium ion batteries achieved great commercial success in electronic consumables, their energy density is yet inadequate to meet the requirement of more sophisticated applications, e.g. electronic vehicles or hybrid electronic vehicles. Metal/air batteries with utilization of O₂ cathode therefore come into considerations due to high working potentials (strong oxidation ability of oxygen) and high specific capacities (total 4 exchanged electrons per oxygen for full oxygen reduction).¹ The Oxygen Reduction Reaction (ORR) is also of prime importance in fuel cells. In both metal/air batteries and fuel cells, the intrinsic sluggish ORR is the rate-determining factor. Although precious metals are the most active electrocatalysts for the ORR,²⁻⁴ the practical applications of precious metals are significantly retarded by high costs and limited availability. Therefore, development of non-precious electrocatalysts with applicable ORR activity is of importance.⁵ By far, carbon,⁶⁻¹⁰ polymer,¹¹⁻¹⁴ nitrides,¹⁵⁻¹⁶ transitional metals and oxides/sulphates¹⁷⁻²⁶ were reported to be effective non-precious

electrocatalysts for the ORR. Among the above non-precious candidates, Mn-based oxides have been intensively investigated due to low cost, biocompatibility, resource abundance and appreciable ORR activity in alkaline media.²⁷⁻³¹ However, to be successfully implemented, further improvement in ORR activity of Mn-based oxides is urgently needed.

Several strategies can be introduced to enhance ORR activity of electrocatalysts. Nanostructured materials generally possess enhanced kinetics and activity to the corresponding bulk counterparts due to high surface area, high surface energies and unique size effects.³²⁻³³ Simultaneously, nanomaterials tend to exhibit inferior durability and inconvenient side reactions. Therefore, micro/nano hierarchical architectures are intriguing on combining merits of nanoscaled materials on high activity and micron-sized materials on high stability.^{10, 34} Secondly, porous structures could provide more electrochemical interfaces and effective channels for mass transfer, favorable for catalytic reactions.³⁵⁻³⁶ Another strategy involves in introducing foreign species into manganese oxide backbones with the formation of physical-level heterostructures or chemical-level mixtures. In the former, enhanced catalytic capabilities could be expected due to the synergetic combination of multiple functionalities from individual components and also unusual physicochemical properties of the heterojunctions.^{9, 14, 17, 22-23, 25, 29, 37} In the latter, the in-lattice introduction of foreign species with the formation of new phases could significantly alter surface chemistry of manganese oxide matrix and therefore provide unprecedented opportunities on tailoring the catalytic capabilities.^{8, 19, 38-40}

The main challenge for above approaches lies in the yet

limited number of synthetic routes for controlled synthesis of porous hierarchical Mn-based compositing oxides and unambiguous specification on structure-activity relationships. Herein, we report a modified solvothermal approach for preparation of compositing carbonates between Mn and X (X = Co, Ni and Fe). Upon a post annealing treatment, the aforementioned carbonates are transformed into the corresponding micro/nano hierarchical structured mixed oxides with increase in porosity. Special attentions are focused on the influence of the compositing manner on the microstructure of the mixed oxides. It is found that onion-like core-shell architectures appear in the Mn-Co and Mn-Ni systems due to the volume shrinkage arisen from the generation of chemical-level mixed oxides. While less porous structure occurs in the Mn-Fe system with the formation of a physical-level mixture. The ORR activity of the prepared compositing oxides in alkaline media are investigated by using voltammetry in different hydrodynamic situations. An enhanced ORR activity is observed in Mn-Co mixed oxide, which is rationalized in terms of the unique microstructure and crystallographic phase. The present study suggests that proper mixing is an effective method on activating ORR activity of manganese oxides, which is beneficial to developing non-precious electrocatalysts for fuel cells and metal/air batteries.

Experimental section

Materials Synthesis

All chemical reagents are of analytical grade from Aldrich and were used without further purification. A modified solvothermal process was employed herein with the change of Mn precursors from MnCl_2 to KMnO_4 .⁴¹ In a typical synthesis, 1 mmol KMnO_4 was added into 40 mL ethylene glycol containing 2 mmol XCl_n ($\text{XCl}_n = \text{CoCl}_2$, FeCl_3 or NiCl_2) under magnetic stirring. After the component was well distributed, 30 mmol urea was added. The mixture was then transferred into a Teflon-lined stainless steel autoclave with a capacity of 100 mL before 40-min magnetic stirring. The autoclave was then sealed and treated at 200 °C for 10 h. Then the solvothermal samples were obtained after centrifugation (7000 rpm) and washed several times by deionized water and alcohol to remove possible impurities, followed by drying in air at 80 °C. As precursors, the obtained solvothermal samples were heated under 600 °C in a furnace for 12 h in air with a heating rate of 5 °C per minute before the final black product was obtained. For comparison, similar preparation with the absence of XCl_n was also conducted in purpose of preparing manganese oxides.

Materials Characterization

The crystallographic characters of the obtained samples were investigated with powder X-ray diffraction (XRD; Shimadzu XRD-6000, Cu $K\alpha$, $\lambda = 1.5406 \text{ \AA}$) at a scanning rate of 2 degree min^{-1} . The morphology of the as-prepared samples was examined with field-emission scanning electron microscopy (SEM; FEI Sirion field emission) and transmission electron microscopy (HRTEM, Philips FEG CM300, 300 kV). Elemental compositions of the prepared samples were measured with energy dispersive X-ray spectroscopy (EDX, EDAX GENESIS 7000) analysis coupled with SEM. Thermal behaviors of samples were examined by thermogravimetric analysis (TGA, Shimadzu DTG-

60) from room temperature up to 800 °C at a heating ramp of 5 °C min^{-1} in air. N_2 adsorption/desorption isotherms at 77 K were used to determine specific surface area and pore-size distribution of all samples (Micromeritics ASAP 2020). All the prepared samples were degassed at 180 °C prior to nitrogen adsorption measurements. The Brunauer-Emmett-Teller (BET) specific surface area was determined by a multipoint BET method using the adsorption data in the relative pressure (P/P_0) range of 0.05-0.3. The adsorption isotherms were employed to determine the pore-size distribution using the Barret-Joyner-Halender (BJH) method, assuming a cylindrical pore model. The electrical conductivity of the annealed samples was tested over the corresponding pellets (10 mm in diameter) prepared from die-pressing in 8 MPa by using the 4-probe method (Suzhou JG, SZT-B).

Electrochemical Measurement

Electrochemical measurements of the annealed samples for ORR were recorded by using an Autolab electrochemical workstation (PGSTAT128N) at room temperature in a three-electrode system using 0.1 M KOH as the electrolyte, Pt wire (1 mm in diameter, CHI) as the counter electrode and reversible hydrogen electrode (RHE) in the same electrolyte as the reference electrode. The working electrode was sample-modified glassy carbon (GC) disk electrode with a diameter of 5 mm. For preparation of the working electrode, 4 mg of the prepared samples and 1 mL 0.2% Nafion/ethanol solution were dispersed into a 5 mL vial by ultrasonication to form a homogenous dispersion of the samples. Then 16 μL of the suspension was pipetted out and casted onto the glassy carbon disk electrode. Cyclic voltammetric (CV) measurements were recorded at a scan rate of 50 mV s^{-1} . Linear sweep voltammetry (LSV) by using a rotating glassy carbon disk electrode (RDE, 4 mm in diameter) at a rotating rate of 1600 rpm was recorded at a scan rate of 5 mV s^{-1} . Prior to measurement, O_2 was bubbled directly into the cell for at least 30 min to saturate the solution. During each measurement, O_2 was flushed over the cell solution.

Results and Discussion

Compared with hydrothermal synthesis, solvothermal preparation is beneficial to restraining overgrowth of nuclei and sophisticated control the growth process due to the higher viscosity of organic solvents. In the present study, KMnO_4 instead of Mn(II) species is employed as the Mn precursor, which can directly react with the employed solvent, i.e. ethylene glycol.⁴² While the Mn(II) species and XCl_n ($\text{XCl}_n = \text{CoCl}_2$, FeCl_3 or NiCl_2) cannot directly react with the ethylene glycol, with ethylene glycol being adsorbed on the surface of crystals.

With the addition of urea and heating treatment, all the metal species tend to transform into metal carbonates. The generation of carbonates is confirmed by the XRD patterns of the solvothermal products. As shown in Fig. 1a, all the XRD patterns of the solvothermal products can be indexed with MnCO_3 (JCPDS No. 44-1472, rhombohedral, Space Group: R-3c). In the following discussion, the solvothermal samples are represented as Mn-C-O and Mn-X-C-O. The characteristic diffraction peaks from the X-based carbonates are absent in the corresponding patterns due to the slower nucleation rates of X-based carbonates. It is found that

the crystallinity of the Mn-C-O samples is higher than those of Mn-X-C-O. This is also due to the higher reaction rate of KMnO_4 than XCl_n . The introduction of X species tends to restrain the nucleation of MnCO_3 due to the competitive formation of carbonates between Mn and X species. A slight deviation of the diffraction peaks from MnCO_3 appears in the Mn-Co-C-O sample, indicating the chemical mixing process in the sample.

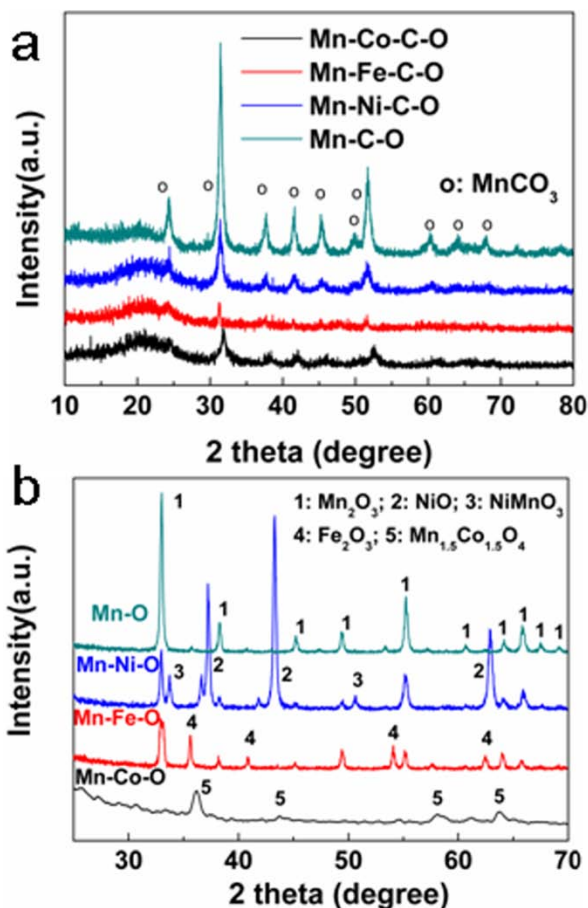


Fig. 1 XRD patterns of the solvothermal samples before (a) and after (b) annealing at 600 centigrade for 12 h in air.

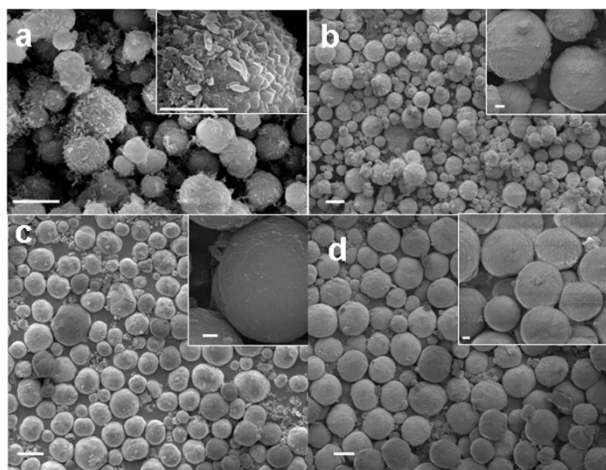


Fig. 2 SEM images of the solvothermal Mn-C-O (a), Mn-Co-C-O (b), Mn-Ni-C-O (c) and Mn-Fe-C-O (d). The scale bars in the figures and insets represent 5 μm and 1 μm , respectively.

The microstructure of the solvothermal samples were then characterized by SEM. As shown in Fig. 2, all the samples consist of microspheres. The present ethylene glycol and derived polymers can function as capping agents during synthesis, which tends to be radially adsorbed on the surface of nuclei and facilitates the formation of spherical morphology. The diameter of the prepared Mn-C-O microspheres ranges from 3 and 5 μm , while larger-sized Mn-X-C-O (ranging from 5 and 8 μm) microspheres were generated. The different size of the samples can be addressed by the discrepancy in reaction capability between KMnO_4 and XCl_n in the system. It is speculated that, in the compositing system, Mn-species first nucleate. And X-species then precipitate onto the Mn-species, leading to the larger size of the compositing samples than the Mn-C-O. As shown in Fig. 2a, well shaped crystals occur in the Mn-C-O. While the Mn-X-C-O samples are poor crystalline and featureless in shape. The higher crystalline Mn-C-O than the Mn-X-C-O can be ascribed to the higher reactivity of KMnO_4 .

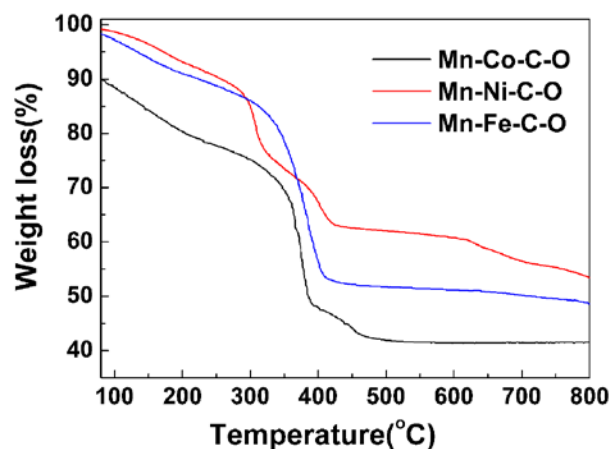


Fig. 3 TGA curves of the compositing carbonates obtained from solvothermal preparation.

Fig. 3 displays the TGA curves in air of the compositing carbonates. Minor weight loss below 200 $^{\circ}\text{C}$ can be assigned to the loss of physically adsorbed or chemically bonded water. At temperature higher than 300 $^{\circ}\text{C}$, phase transformation from carbonates to oxides occurs, with the occurrence of substantial weight loss. Only one weight-loss peak appears in the TGA curve of Mn-Fe-C-O; while multiple peaks occur in the curves of Mn-Co-C-O and Mn-Ni-C-O. Such difference in TGA curves indicates the discrepancy in reaction mechanisms. For all the compositing samples, the weight loss becomes stabilized after 500 $^{\circ}\text{C}$. Therefore, the annealing temperature of the carbonates for preparation of oxides is fixed to 600 $^{\circ}\text{C}$.

The solvothermal samples were then annealed at 600 $^{\circ}\text{C}$ for 12 h in air. Fig. 1b displays the XRD patterns of the annealed samples. As can be seen, the previously obtained carbonates are transformed into oxides after annealing due to the elimination of carbon and organic species. Therefore, the annealed samples are notated as Mn-O and Mn-X-O in the following. As shown in Fig. 1b, the Mn-O sample is pure Mn_2O_3 (JCPDS No. 41-1442, cubic, Space Group: $Ia-3$). The Mn-Ni-O sample consists of Mn_2O_3 , NiO (JCPDS No. 47-1049, cubic, Space Group: $Fm-3m$) and NiMnO_3 (JCPDS No. 48-1330, rhombohedral, Space Group: $R-3$).

The Mn-Fe-O sample is constituted by Fe_2O_3 (JCPDS No. 33-0664, rhombohedral, Space Group: R-3c) and Mn_2O_3 . For the Mn-Co-O sample, the corresponding XRD pattern can be well indexed with the face-centered-cubic $\text{Mn}_x\text{Co}_{3-x}\text{O}_4$ (JCPDS No. 23-1237, cubic, Space Group: Fd-3m) phase.^{19, 41} EDX was employed to determine the chemical compositions of the annealed samples. The molar ratios of Mn/X in the Mn-X-O samples are observed as 1.05 (Mn/Co), 9.10 (Mn/Ni) and 0.75 (Mn/Fe) for the Mn-Co-O, Mn-Ni-O and Mn-Fe-O samples, respectively. Therefore, the Mn-Co-O should be cubic spinel $\text{Mn}_{1.5}\text{Co}_{1.5}\text{O}_4$.^{19, 41} The chemical compositions of the annealed samples are inconsistent with the stoichiometric value in the precursors (Mn/X=0.5) due to the different reaction capability of Mn and X species. For example, Co cations tend to coordinate with NH_3 derived from urea, which retards the precipitation of Co species.⁴¹

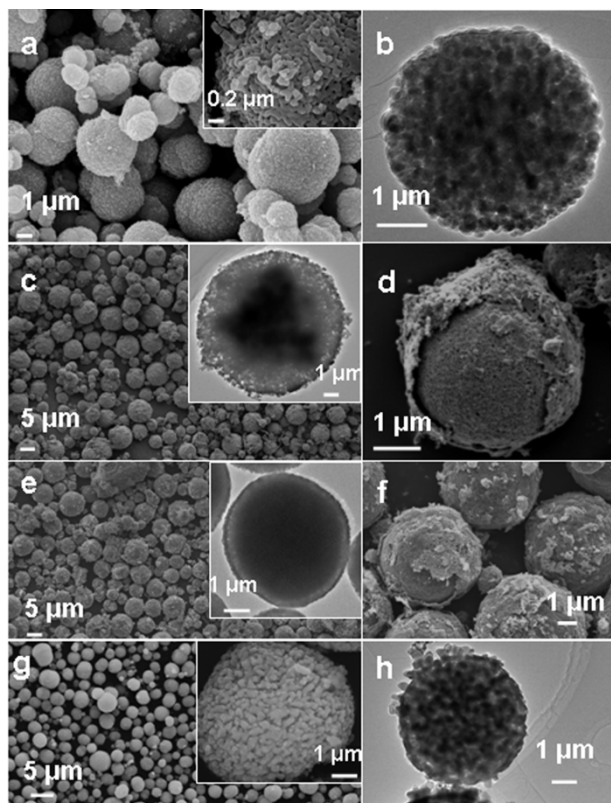


Fig. 4 SEM and TEM images of the annealed Mn-O (a and b), Mn-Co-O (c and d), Mn-Ni-O (e and f) and Mn-Fe-O (g and h).

Fig. 4 presents the SEM and TEM images of the annealed samples. It is clearly shown that the macroscopical morphology of microspheres is generally retained after annealing, with the size of the microspheres unchanged. Similar morphology of porous microspheres appears in the samples of Mn-O and Mn-Fe-O. Interestingly, the Mn-Co-O and Mn-Ni-O samples exhibit onion-like core-shell microstructure, different with that of Mn-O. It is clearly shown that more voids exist in the two onion-like samples. With the elimination of carbon and organic species, all the annealed samples become more porous. The porous characteristic is further confirmed by nitrogen adsorption/desorption measurements. As exhibited in Fig. 5, all the samples show typical isotherms of type IV with high

adsorption and hysteresis loops occurring at a high relative pressure ranging from 0.8 to 1.0, suggesting the presence of large mesopores and macropores.⁴³ The shape of the hysteresis loops is of type H3, associated with slit-like pores formed by the aggregations of the plate-like particles. The BET specific surface area, pore volume and average pore size data were summarized in Table 1. The Mn-Co-O and Mn-Ni-O sample have larger surface area and pore volume than the Mn-O, with lower surface area and pore volume than Mn-O occurring in Mn-Fe-O.

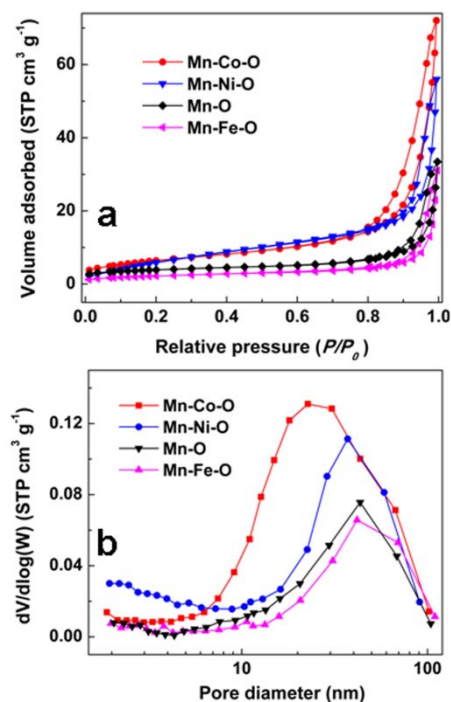


Fig. 5 Nitrogen adsorption/desorption isotherms (a) and corresponding pore-size distribution of the annealed samples.

Table 1 Summary on the Nitrogen adsorption/desorption measurements of the annealed samples

	surface area ($\text{m}^2 \text{g}^{-1}$)	Pore volume ($\text{cm}^3 \text{g}^{-1}$)	Average pore size (nm)
Mn-Co-O	26	0.075	7.6
Mn-Ni-O	24	0.049	12.5
Mn-O	14	0.026	7.7
Mn-Fe-O	8	0.020	10

The different morphology of the annealed samples can be interpreted by the dissimilar mixing manners. Chemical-mixing mechanisms appear in the Mn-Co-O and Mn-Ni-O systems with the formation of new-phase cubic spinel $\text{Mn}_{1.5}\text{Co}_{1.5}\text{O}_4$ and rhombohedral NiMnO_3 . Such an in-lattice chemical mixing process incurs the further shrinkage of the microspheres and facilitates the formation of onion-like core-shell microstructure. The further shrinkage of the chemical-mixing samples lead to the observed higher specific surface area and pore volume of the Mn-Co-O and Mn-Ni-O samples than those of Mn-O. Incomplete chemical-mixing in the Mn-Ni-O with the co-presence of Mn_2O_3 , NiO and NiMnO_3 leads to lower specific surface area and pore volume of the Mn-Ni-O than those of Mn-Co-O. In the latter, complete chemical-mixing mechanism is predominant with the formation of phase-pure cubic spinel $\text{Mn}_{1.5}\text{Co}_{1.5}\text{O}_4$. In contrast,

physical mixing mechanisms occur in the Mn-Fe-O sample, with the co-presence of Fe₂O₃ and Mn₂O₃. Therefore, lower specific surface area and pore volume than those of Mn-O appear in the Mn-Fe-O sample due to the higher density of Fe₂O₃ (5.24 g cm⁻³) than Mn₂O₃ (4.50 g cm⁻³). The above results highlight the influence of the compositing manner on the microstructure of the mixed oxides, confirming that chemical mixing is favorable for the generation of more porous microstructure. The different mixing mechanism of the studied composites is in agreement with the TGA curves shown in Fig. 3. The formation of chemical-level mixtures in Mn-Co and Mn-Ni systems incurs the multiple weight loss peaks.

Table 2 Electrical resistivity of the annealed samples derived from the 4-probe method

	Mn-Co-O	Mn-Ni-O	Mn-O	Mn-Fe-O
Electrical resistivity (kΩ cm)	20.6	22.5	23.1	10.8

The electrical resistivity of the annealed samples was characterized by using the 4-probe method. As listed in Table 2, all the Mn-X-O samples have a lower resistivity than that of the Mn-O sample, suggesting the mixing process is beneficial to decreasing ohmic polarizations of manganese oxides. It is also indicated that manganese oxides show higher intrinsic resistivity than that of other oxides.

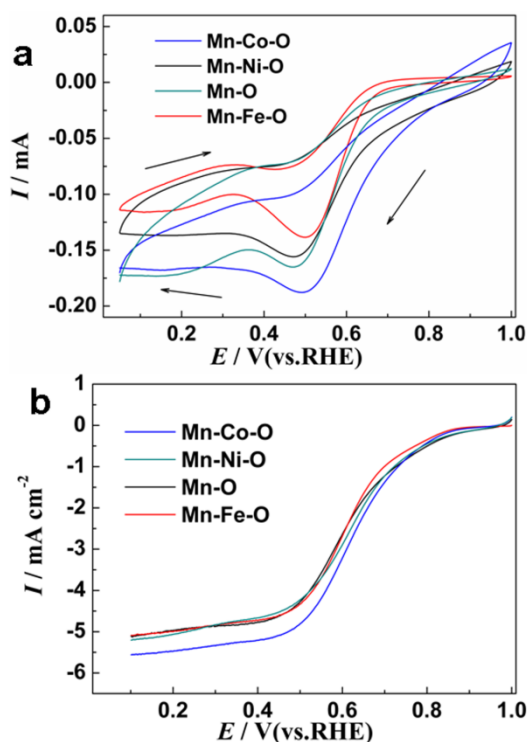


Fig. 6 Cyclic voltammograms recorded at 50 mV s⁻¹ (a) and linear sweep voltammograms recorded by using a rotating-disk-electrode configuration with a rotation speed of 1600 rpm and a scan rate of 5 mV s⁻¹ (b) for the annealed samples-modified GC electrodes in an O₂-saturated 0.1 M KOH solution.

The electro-catalytic activity of all the annealed samples for the ORR is studied by cyclic voltammetry (CV) and linear sweep

voltammetry (LSV) by using a rotating-disk-electrode (RDE) configuration. Fig. 6a displays the static CVs of the annealed samples/glassy carbon (GC) electrodes in O₂-saturated aqueous KOH solution (0.1M) at a scan rate of 50 mV s⁻¹. CVs recorded in the corresponding N₂-saturated electrolyte were also studied (not shown). Such CVs display featureless plots, representing the typical behaviors of charge/discharge currents from electrical double layers. As shown in Fig. 6a, significant cathodic currents appears in the CVs when the electrolyte is saturated with O₂, with the formation of well-defined cathodic peaks ascribed to electrocatalytic oxygen reduction over the annealed samples. More positive onset potentials appear in the Mn-Co-O and Mn-Ni-O samples, indicating higher ORR activity of the two samples. Such an enhancement is believed to be relevant to the onion-like microstructure. The volume shrinkage derived from the formation of chemical mixing renders the higher specific surface area and higher pore volume, therefore leading to higher activity and enhanced mass transfer. While the Mn-Fe-O exhibits a more negative onset potential for ORR and smaller peak current, indicating the inferior ORR activity of the Mn-Fe-O sample. Although the Mn-Fe-O has the lowest electrical resistivity, its lowest specific surface area and pore volume cause the low activity and retarded mass transfer of the sample. The Mn-Fe-O sample consists of physical mixing between Fe₂O₃ (major) and Mn₂O₃, in which Fe₂O₃ possesses intrinsically inferior ORR activity to manganese oxides, nickel oxides and cobalt oxides. It is also speculated that the synergetic effects and contribution from heterojunctions are absent in the Mn-Fe-O sample.

To eliminate the influence of hydrodynamic conditions on evaluation of the intrinsic ORR capability of the samples, a rotating-disk-electrode (RDE) configuration is also utilized to compare the kinetics of ORR for the samples. The technique of RDE is advantageous to exclude the effect of mass transfer and therefore is more reliable to assess the intrinsic ORR kinetics. Fig. 6b shows the LSVs recorded by using a rotating-disk-electrode configuration with a rotation speed of 1600 rpm and a scan rate of 5 mV s⁻¹ for all the annealed samples-modified GC electrodes in an O₂-saturated 0.1 M KOH solution. A significantly higher limiting current density occurs in the Mn-Co-O sample, with the same lower limiting current density appearing in the other three samples. It is also shown that the onset potential of ORR for the Mn-Co-O is more positive than that of the other three samples. The above results confirm the enhanced electrocatalytic ORR activity of the Mn-Co-O sample.

The enhanced electrocatalytic ORR capability of the Mn-Co-O sample can be assigned to its unique crystallographic structure and microstructure. As confirmed above, the prepared Mn-Co-O is phase-pure cubic spinel Mn_{1.5}Co_{1.5}O₄. A recent innovation on non-precious electrocatalysts highlighted the superior electrocatalytic activity of cubic spinel Mn-Co-O nanocrystalline due to the abundant defects increasing oxygen binding ability on the catalyst surface.¹⁹ The formation of chemical mixing in the Mn-Co-O renders the formation onion-like core-shell microspheres with high specific surface area and high pore volume, further enhancing the ORR activity and kinetics. Our finding suggests that tailoring the crystal phase and microstructure could be effective routes for activating the activity of non-precious electrocatalysts for the ORR, which adds new

knowledge on developing non-precious electrocatalysts for fuel cells and metal/air batteries.

Conclusions

In summary, a modified solvothermal method combined with post annealing treatment with the utilization of KMnO_4 as the Mn precursors was reported here for preparation of porous hierarchical Mn-X (X= Co, Ni and Fe) compositing oxides. It was found that the solvothermally derived metal carbonates microspheres were transformed into the corresponding more porous hierarchical compositing oxides. The results highlighted the influence of the compositing manner on the microstructure of the generated mixed oxides. The generation of chemical-level mixed oxides, viz. phase-pure cubic spinel $\text{Mn}_{1.5}\text{Co}_{1.5}\text{O}_4$ and partial NiMnO_3 in the Mn-Co and Mn-Ni systems facilitated the occurrence of onion-like core-shell architectures with high specific surface area and pore volume due to the volume shrinkage during chemical mixing. While less porous structure occurred in the Mn-Fe system with the formation of a physical-level mixture. Electrochemical characterization in different hydrodynamic situations suggested a significant enhanced ORR activity in alkaline media of the prepared cubic spinel $\text{Mn}_{1.5}\text{Co}_{1.5}\text{O}_4$. The vast difference in ORR activity of all the Mn-X-O samples was rationalized in terms of microstructure and crystallographic phase. This finding added to our understanding of non-precious electrocatalysts and further development of cost-affordable and high-performance alkaline polymer electrolyte fuel cells and metal/air batteries.

Acknowledgements

Financial supports from the Wuhan University (Start-Up Grant and 121075), Excellent-Teacher-Team-Building Scientific Research Project of Hubei University of Education (2012K103), Outstanding Young Talent Project of Hubei Provincial Department of Education (Q20143001), Open Fund of Key Laboratory of Hubei Province of Implantation of Anticancer Active Substances Purification and Application, and NSFC (21203141 and 21303045) are acknowledged. This project was also funded by the Fund for Fostering Talents in Basic Science of the National Natural Science Foundation of China (J1103409).

Notes and references

^a School of Resource and Environmental Sciences, Wuhan University, Wuhan 430072, PR China. Fax: +86 27 68775799; Tel: +86 27 68775799; E-mail: gabrielxiao@whu.edu.cn

^b College of Chemistry and Life Science, Hubei University of Education, Wuhan 430205, PR China. E-mail: twu@whu.edu.cn

- G. Girishkumar, B. McCloskey, A. C. Luntz, S. Swanson and W. Wilcke, *J. Phys. Chem. Lett.*, 2010, **1**, 2193-2203.
- J. Greeley, I. E. L. Stephens, A. S. Bondarenko, T. P. Johansson, H. A. Hansen, T. F. Jaramillo, J. Rossmeisl, I. Chorkendorff and J. K. Nørskov, *Nat. Chem.*, 2009, **1**, 552-556.
- B. Y. Xia, H. B. Wu, X. Wang and X. W. Lou, *J. Am. Chem. Soc.*, 2012, **134**, 13934-13937.
- E. Antolini, *Energy Environ. Sci.*, 2009, **2**, 915-931.
- Y. Zheng, Y. Jiao, M. Jaroniec, Y. G. Jin and S. Z. Qiao, *Small*, 2012, **8**, 3550-3566.
- K. Gong, F. Du, Z. Xia, M. Durstock and L. Dai, *Science*, 2009, **323**, 760-764.
- Y. Jiao, Y. Zheng, M. Jaroniec and S. Z. Qiao, *J. Am. Chem. Soc.*, 2014, **136**, 4394-4403.
- J. Liang, X. Du, C. Gibson, X. W. Du and S. Z. Qiao, *Adv. Mater.*, 2013, **25**, 6226-6231.
- Y. G. Li, W. Zhou, H. L. Wang, L. M. Xie, Y. Y. Liang, F. Wei, J. C. Idrobo, S. J. Pennycook and H. J. Dai, *Nat. Nanotechnol.*, 2012, **7**, 394-400.
- L. F. Wu, H. B. Feng, M. J. Liu, K. X. Zhang and J. H. Li, *Nanoscale*, 2013, **5**, 10839-10843.
- R. Bashyam and P. Zelenay, *Nature*, 2006, **443**, 63-66.
- B. Winther-Jensen, O. Winther-Jensen, M. Forsyth and D. R. MacFarlane, *Science*, 2008, **321**, 671-674.
- G. Wu, K. L. More, C. M. Johnston and P. Zelenay, *Science*, 2011, **332**, 443-447.
- Q. Lu and Y. K. Zhou, *Funct. Mater. Lett.*, 2010, **3**, 89-92.
- Y. Z. Dong, Y. M. Wu, M. J. Liu and J. H. Li, *ChemSusChem*, 2013, **6**, 2016-2021.
- M. J. Liu, Y. Z. Dong, Y. M. Wu, H. B. Feng and J. H. Li, *Chem.-Eur. J.*, 2013, **19**, 14781-14786.
- Y. Y. Liang, Y. G. Li, H. L. Wang, J. G. Zhou, J. Wang, T. Regier and H. J. Dai, *Nat. Mater.*, 2011, **10**, 780-786.
- G. Q. Zhang, B. Y. Xia, C. Xiao, L. Yu, X. Wang, Y. Xie and X. W. Lou, *Angew. Chem.-Int. Edit.*, 2013, **52**, 8643-8647.
- F. Y. Cheng, J. A. Shen, B. Peng, Y. D. Pan, Z. L. Tao and J. Chen, *Nat. Chem.*, 2011, **3**, 79-84.
- S. Lu, J. Pan, A. Huang, L. Zhuang and J. Lu, *Proc. Natl. Acad. Sci. U. S. A.*, 2008, **105**, 20611-20614.
- M. Lefevre, E. Proietti, F. Jaouen and J.-P. Dodelet, *Science*, 2009, **324**, 71-74.
- J. J. Duan, Y. Zheng, S. Chen, Y. H. Tang, M. Jaroniec and S. Z. Qiao, *Chem. Commun.*, 2013, **49**, 7705-7707.
- G. Q. Zhang, B. Y. Xia, X. Wang and X. W. Lou, *Adv. Mater.*, 2014, **26**, 2408-2412.
- W. Xiao, D. Wang and X. W. Lou, *J. Phys. Chem. C*, 2009, **114**, 1694-1700.
- H. L. Wang, Y. Y. Liang, Y. G. Li and H. J. Dai, *Angew. Chem.-Int. Edit.*, 2011, **50**, 10969-10972.
- Y. Y. Liang, H. L. Wang, J. G. Zhou, Y. G. Li, J. Wang, T. Regier and H. J. Dai, *J. Am. Chem. Soc.*, 2012, **134**, 3517-3523.
- Q. W. Tang, L. H. Jiang, J. Liu, S. L. Wang and G. Q. Sun, *ACS Catal.*, 2014, **4**, 457-463.
- F. Y. Cheng, Y. Su, J. Liang, Z. L. Tao and J. Chen, *Chem. Mater.*, 2010, **22**, 898-905.
- Y. Gorlin, C. J. Chung, D. Nordlund, B. M. Clemens and T. F. Jaramillo, *ACS Catal.*, 2012, **2**, 2687-2694.
- F. Cheng, J. Shen, W. Ji, Z. Tao and J. Chen, *ACS Appl. Mater. Interfaces*, 2009, **1**, 460-466.
- K. L. Pickrahn, S. W. Park, Y. Gorlin, H.-B.-R. Lee, T. F. Jaramillo and S. F. Bent, *Adv. Energy Mater.*, 2012, **2**, 1269-1277.
- W. Chen and S. W. Chen, *Angew. Chem. Int. Ed.*, 2009, **48**, 4386-4389.
- A. S. Arico, P. Bruce, B. Scrosati, J.-M. Tarascon and W. van Schalkwijk, *Nat Mater*, 2005, **4**, 366-377.
- Y. S. Ding, X. F. Shen, S. Gomez, H. Luo, M. Aindow and S. L. Suib, *Adv. Funct. Mater.*, 2006, **16**, 549-555.
- X. W. Lou, L. A. Archer and Z. C. Yang, *Adv. Mater.*, 2008, **20**, 3987-4019.
- L. Z. Wang, F. Q. Tang, K. Ozawa, Z. G. Chen, A. Mukherj, Y. C. Zhu, J. Zou, H. M. Cheng and G. Q. Lu, *Angew. Chem.-Int. Edit.*, 2009, **48**, 7048-7051.
- S. E.-D. Mohamed and O. Takeo, *Angew. Chem. Int. Ed.*, 2006, **45**, 5963-5966.
- C. Z. Yuan, H. B. Wu, Y. Xie and X. W. Lou, *Angew. Chem.-Int. Edit.*, 2014, **53**, 1488-1504.
- F.-P. Hu, X.-G. Zhang, F. Xiao and J.-L. Zhang, *Carbon*, 2005, **43**, 2931-2936.
- K. Cheng, F. Yang, G. L. Wang, J. L. Yin and D. X. Cao, *J. Mater. Chem. A*, 2013, **1**, 1669-1676.
- J. F. Li, S. L. Xiong, X. W. Li and Y. T. Qian, *J. Mater. Chem.*, 2012, **22**, 23254-23259.

42. W. Xiao, J. S. Chen and X. W. Lou, *CrystEngComm*, 2011, **13**, 5685-5687.
43. M. Kruk and M. Jaroniec, *Chem. Mater.*, 2001, **13**, 3169-3183.

5

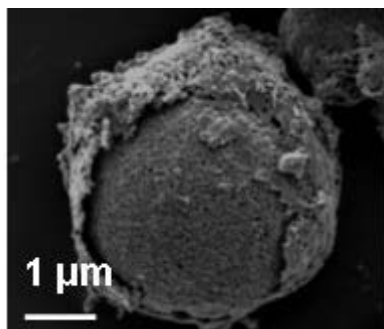
10

TOC:

15

20

25



Porous cubic spinel $\text{Mn}_{1.5}\text{Co}_{1.5}\text{O}_4$ with onion-like core-shell microstructure were prepared, which showed enhanced electrocatalytic activity towards oxygen reduction.